5G PDSCH: PERFORMANCE ANALYSIS OF DMRS AND PTRS DESIGNS FOR CHANNEL AND PHASE NOISE ESTIMATION IN MM-WAVE

A THESIS SUBMITTED TO
THE GRADUATE SCHOOL OF ENGINEERING AND SCIENCE
OF BILKENT UNIVERSITY
IN PARTIAL FULFILLMENT OF THE REQUIREMENTS FOR
THE DEGREE OF
MASTER OF SCIENCE
IN
ELECTRICAL AND ELECTRONICS ENGINEERING

By
Doğan Kutay Pekcan
August 2021

5G PDSCH: Performance Analysis of DMRS and PTRS Designs for Channel and Phase Noise Estimation in mm-Wave
By Doğan Kutay Pekcan
August 2021

We certify that we have read this thesis and that in our opinion it is fully adequate, in scope and in quality, as a thesis for the degree of Master of Science.

Sinan Gezici (Advisor)

Nail Akar

Tolga Girici

Approved for the Graduate School of Engineering and Science:

Ezhan Karaşan
Director of the Graduate School

ABSTRACT

5G PDSCH: PERFORMANCE ANALYSIS OF DMRS AND PTRS DESIGNS FOR CHANNEL AND PHASE NOISE ESTIMATION IN MM-WAVE

Doğan Kutay Pekcan
M.S. in Electrical and Electronics Engineering
Advisor: Sinan Gezici
August 2021

The mm-Wave is one of the main enablers for the performance requirements of 5G. Although it provides communication systems with huge bandwidth and data rates, it also has some disadvantages as the carrier frequencies can significantly exceed 6 GHz and go up to 300 GHz. For example, there are significant challenges such as propagation loss and severe phase noise (PN). The PN can be observed in two parts: common phase error (CPE) and inter-carrier interference (ICI). In the literature, there are algorithms for the estimation and compensation of PN for OFDM-based systems. We apply both CPE and ICI compensation algorithms for 5G PDSCH at the carrier frequency of 70 GHz. Detailed performance analysis is performed for demodulation reference signal (DMRS) based channel estimation and phase-tracking reference signal (PTRS) based PN estimation. We observe the effects of different reference signal parameters in 5G for each PN compensation algorithm. For this purpose, we use up-to-date power spectral density (PSD) models for PN modeling and show uncoded bit error rate (BER) graphs obtained via extensive simulations for MATLAB's tapped delay line (TDL) channels. We also analyze the system performance under very high Doppler, where PTRS based channel estimation is compared with DMRS based channel estimation.

Keywords: 5G, mm-Wave, DMRS, PTRS, channel estimation, phase noise.

ÖZET

5G PDSCH: MM-DALGA İÇİN KANAL VE FAZ GÜRÜLTÜSÜ KESTİRİMİNDE DMRS VE PTRS TASARIMLARININ PERFORMANS ANALİZİ

Doğan Kutay Pekcan
Elektrik ve Elektronik Mühendisliği, Yüksek Lisans
Tez Danışmanı: Sinan Gezici
Ağustos 2021

5G ile birlikte gelen performans gereksinimlerinin temel sağlayıcılarından birisi olarak mm-dalga gösterilebilir. mm-dalga teknolojisi, çok yüksek bant genişliği ve veri hızları sağlamakla birlikte, taşıyıcı frekansın 6GHz'den 300 GHz değerlerine kadar çıkabilecek olmasından dolayı bazı dezavantajları da beraberinde getirmektedir. Örneğin, yayılım kaybı ve şiddetli faz gürültüsü gibi önemli zorluklar bulunmaktadır. Faz gürültüsü, ortak faz hatası (CPE) ve taşıyıcılar arası girişim (ICI) olmak üzere iki temel etkiden oluşur. Literatürde, OFDM tabanlı iletişim sistemleri için, faz gürültüsü kestirimi ve dengelenmesi amacıyla birçok algoritma bulunmaktadır. Bu tezde, CPE ve ICI etkileri için ayrı ayrı olmak üzere, 5G aşağı yönlü paylaşım kanalı (PDSCH) için, 70 GHz taşıyıcı frekansında faz gürültüsü kestirimi ve dengelenmesi için algoritmalar kullanılmaktadır. Demodülasyon referans sinyali (DMRS) ve faz takip referans sinyali (PTRS) tabanlı kanal ve faz gürültüsü kestirimleri uygulanarak performans sonuçları elde edilmektedir. 5G için referans sinyal parametreleri ve numeroloji kullanımının performans sonuçları üzerindeki etkisi gözlemlenmektedir. Bu amaçla, faz gürültüsü modellemesi için osilatör spektral güç yoğunluğu (PSD) referans alınarak, MATLAB gecikme yayılımlı kanalları için kodlamasız bit hata oranı (BER) grafikleri elde edilmektedir. Son olarak, yüksek Doppler senaryoları ele alınarak, PTRS ve DMRS tabanlı kanal kestirim sonuçları karşılaştırılmaktadır.

Anahtar sözcükler: 5G, mm-Dalga, DMRS, PTRS, kanal kestirimi, faz gürültüsü.

Acknowledgement

Firstly, I would like to show my great appreciation for my advisor Prof. Sinan Gezici. He was very encouraging and supportive throughout my graduate studies. I really appreciate him for being very understanding and patient, and I feel very lucky that I was able to ask even the simplest question without any hesitation.

Secondly, I would like to thank Dr. Çağrı Göken, for his continuous support and guidance through my studies. He helped me to find my way to simplify the problems related to the project that I was working on. I also want to thank my family, my father, and my mother, for their invaluable support and the life experiences they shared with me.

Lastly, I thank all my professors and Bilkent University, as well as my dear friends and colleagues who always believed in me.

This work is supported by ASELSAN Inc. under the "5G Platform" project, which is partly funded by the Scientific and Technological Research Council of Turkey (TUBITAK) under the project number 1160206. I acknowledge that ...

Contents

List of Figures

List of Tables

Chapter 1

Introduction

1.1 Evolution of Mobile Communications, 5G and mm-Wave

During the last few decades, mobile communication has made an immense progress in meeting society's increased demands and new technologies. Starting from the first generation (1G), almost every decade, a new generation of mobile communication has been developed and introduced by the releases of Third Generation Partnership Project (3GPP), eventually evolving into 4G/LTE (Long Term Evolution) [6]. As most of the requirements of 4G are met, the 5th generation (5G) has become the mainstream of most research conducted in the last several years.

5G mobile communication technology, also referred to as new radio (NR), is being standardized by the 3GPP [7]. 5G has started to being standardized for many unique aspects such as to achieve 1 Gbps or higher throughput, ultra-reliable and low latency communications (URLLC), and low energy consumption [8].

The mm-Wave frequency bands can be shown as one of the main aspects of

5G since it is considered as an enabler for the performance requirements of 5G [9]. The mm-Wave spectrum roughly lies in 10 to 300 GHz frequencies, providing much higher bandwidth and bit-rates compared to 4G systems [10].

5G NR standards are grounded by the release 15 (Rel-15) and Rel-16 provided by 3GPP, where carrier frequencies up to 52.6 GHz are supported. 3GPP has decided to further study the requirements for communications above 52.6 to 114.25 GHz [11]. As expected, there are more significant challenges for higher frequencies such as propagation loss, atmospheric absorption, and severe phase noise (PN). Therefore, 3GPP started the Rel-17 study to address the design requirements. The main focus is on supporting the NR frequency range 2 (FR2) with 52.6 to 71 GHz as well, with minimal changes in the previous releases. According to plans, the Rel-17 study is going to be finalized in the second quarter of 2022 [12, 13]. The latest contribution reports regarding the increased PN effect are mainly focused on providing more reliable PN models and possibly improved phase tracking reference signal (PTRS) designs for enhanced PN mitigation.

In the remainder of this thesis, we first explain the 5G numerology and frame structure together with the physical downlink shared channel (PDSCH) and its reference signals. Then, phase noise modeling and orthogonal frequency division multiplexing (OFDM) signal model is derived. Eventually, we present the channel and phase noise estimation algorithms used in this work and present the performance results of the system.

1.2 5G Numerology and Frame Structure

In this section, 5G numerology and frame structure are briefly explained with a detailed illustration. 3GPP agrees that for uplink and downlink transmissions, orthogonal frequency division multiplexing with cyclic prefix (CP-OFDM) waveform is used in 5G [1]. The use of discrete Fourier transform spread OFDM (DFT-S-OFDM) is also supported in some cases. However, in this thesis, CP-OFDM waveform is adopted. General illustration for 5G NR frame structure is shown in Fig. 1.1 [1].

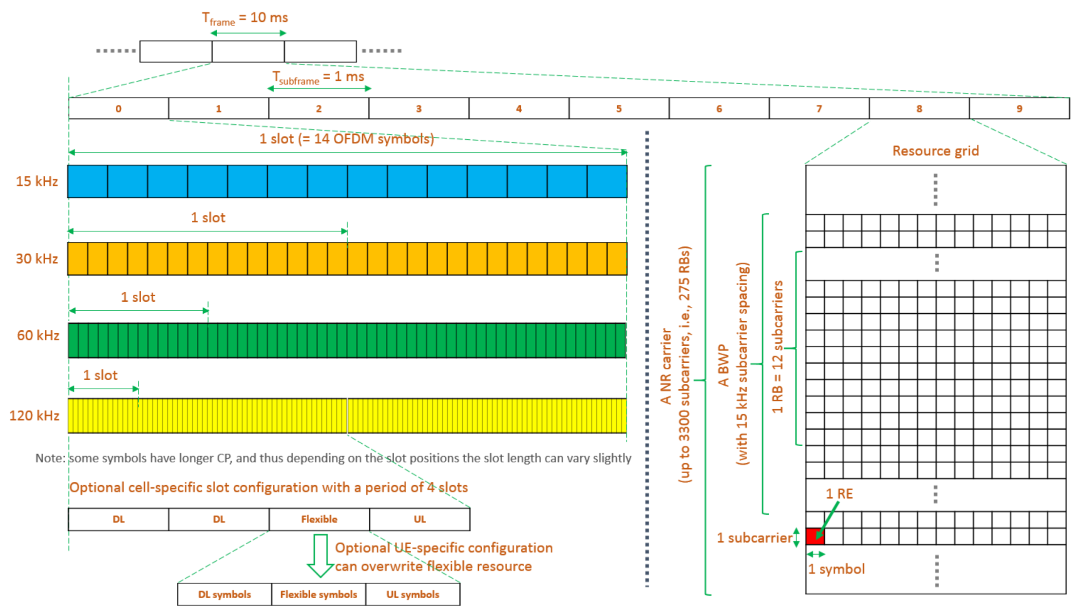

Figure 1.1: 5G NR frame structure [1].

With mm-Wave introduced in 5G NR, two frequency ranges are supported as FR1 and FR2. FR1 is referred to as sub-6 GHz, and it corresponds to 450 MHz – 6 GHz frequencies, whereas FR2 is referred to as mm-Wave and corresponds to 24 GHz – 52.6 GHz frequencies. For above 52.6 GHz, higher subcarrier spacings up to 960 kHz are being considered to be used. This thesis examines the performance for higher subcarrier spacing values such as 240, 480, and 960 kHz at a carrier frequency of 70 GHz.

In NR, flexible subcarrier spacing is introduced. For scaling parameter $\mu \in \{0, 1, 2, 3, 4\}$, subcarrier spacing can take values $2^{\mu} \times 15$ kHz, where the fixed 15 kHz subcarrier spacing in LTE is just scaled, where the CP length of $4.7\,\mu s$ in LTE is also scaled by $2^{-\mu}$. With mm-Wave and increased carrier frequencies, higher subcarrier spacing values become more suitable for use, because, for higher frequencies, channel delay spread tends to be lower, which is suitable for shortened CP length for inter-symbol interference (ISI) to be avoided. On the other hand, phase noise becomes much more problematic for higher frequencies.

5G also introduces “mini-slot" transmission to provide reduced latency and interference scenarios, especially in ultra-reliable low latency communications (URLLC). However, the very typical unit for a 5G transmission is a slot. In this thesis, performance analysis and algorithms are performed over an OFDM grid for a slot transmission.

For a slot-based transmission, the corresponding OFDM grid is composed of subcarriers in the frequency domain and 14 OFDM symbols in time. The number of subcarriers is determined by the used bandwidth and subcarrier spacing values. In a resource grid, each resource element (RE) occupies one subcarrier in frequency and 1 OFDM symbol duration in time. For modulation and coding scheme (MCS), similar to LTE, quadrature amplitude modulation (QAM) of orders 16, 64, and 256 are used together with binary and quadrature phase-shift keying (BPSK/QPSK), where QPSK is mostly used for reference signaling. For data channel and coding, rate compatible quasi-cyclic low-density parity-check (LDPC) codes are used in 5G, which is different from LTE, where turbo codes are used.

1.3 5G Physical Downlink Shared Channel (PDSCH) Structure

Physical downlink shared channel (PDSCH) is the downlink channel in 5G, where the user data, system information, and higher-layer information are transmitted. User data goes through physical-layer processing, where CRC attachment, LDPC encoding, rate matching, and modulation are performed. The process of PDSCH physical-layer processing for each transport block is shown in Fig. 1.2 [1].

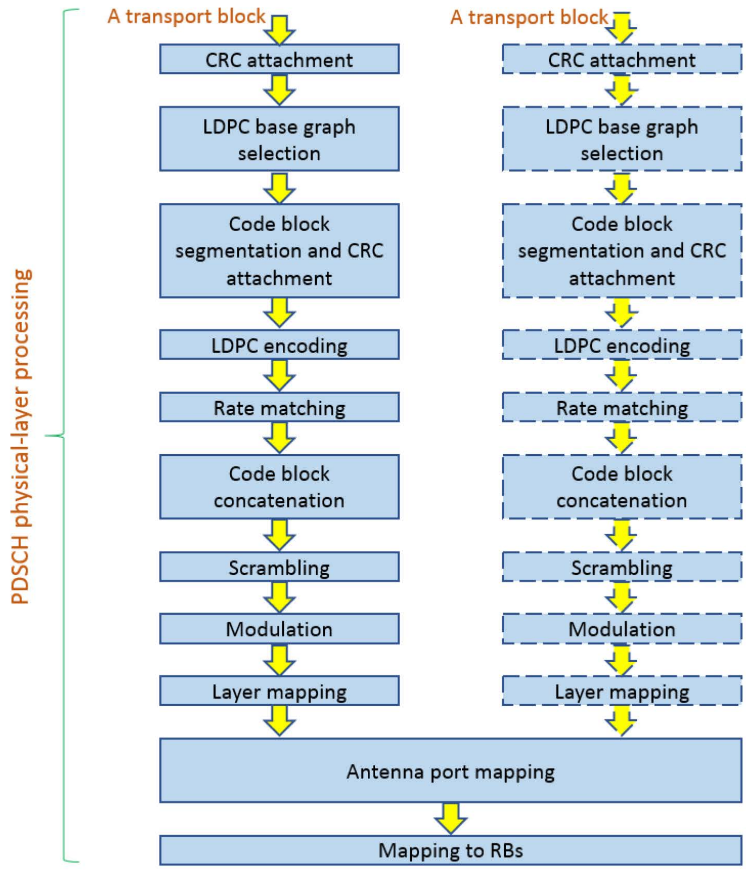

Figure 1.2: 5G PDSCH physical layer processing [1].

Together with the modulated transport block symbols that carry the user data and system information, there are two main reference signals to be transmitted in the PDSCH resource block: DMRS (demodulation reference signal) and PTRS (phase tracking reference signal). DMRS is used for estimating the channel between the transmitter and the receiver. In contrast, the phase of the local oscillator at both the receiver and transmitter is tracked by using PTRS.

1.3.1 Demodulation Reference Signal (DMRS) Structure

The demodulation reference signal (DMRS) consists of the pilot symbols that are transmitted in specified resource elements and used for channel estimation.

In the literature, it is also referred to as pilot-based channel estimation. The number of DMRSs used in a slot and the resource elements dedicated to them are determined by DMRS configuration parameters. Given those configuration parameters and N_{Cell}^{ID}, DMRS symbols are generated by using QPSK modulation on the pseudorandomly generated gold sequences and placed in specified resource elements as determined by 3GPP standards [14].

After performing synchronization, the receiver can perform pilot based channel estimation by regenerating the DMRS symbols [2] as the $N_{\text{Cell}}^{\text{ID}}$ value is known, and it is sufficient for determining the pseudorandomly generated DMRS symbols and the space-time locations of them [15].

1.3.1.1 DMRS for PDSCH

To determine PDSCH DMRS resource allocation, there are four main parameters. DMRS locations and the number of DMRS symbols in a slot are determined accordingly to these parameters as specified in the following:

- *Mapping type*: There are two options for this parameter that are mapping types A and B. For type A, the first occurrence of DMRS happens on the second or third OFDM symbol within a slot. On the other hand, for type B, DMRS is inserted in the very first OFDM symbol within a slot. In this thesis, mapping type A is used.

- *Configuration type*: This parameter determines the DMRS density in the frequency domain. There are two options for this parameter that are configuration types 1 and 2. For type 1, one of each two subcarriers is used for DMRS transmission, whereas for type 2, two consecutive subcarriers of each six subcarriers are used for DMRS transmission. In this thesis, configuration type 1 is used in simulations.

- *Front load*: This parameter defines single or double symbol DMRS use in the time domain for mapping type A. For double symbol DMRS, two consecutive resource elements are used for DMRS along the time domain. In this thesis, the single symbol DMRS is used in simulations.

- *Additional position* (N_{add}^{DMRS}): Additional DMRS position can take values in $\{0, 1, 2, 3\}$ for configuration type 1. For type 1-A transmission, by default, at least one OFDM symbol is used for DMRS transmission (which corresponds to additional position 0). DMRS symbols are inserted to the specified subcarriers in an OFDM symbol within a slot for each additional position.

With orthogonal cover codes for specific DMRS resource allocations, DMRS can support up to 12 orthogonal layers for multiple-input multiple output (MIMO) communication. To illustrate the effects of DMRS configuration parameters, examples are shown in Fig. 1.3 for the different configuration parameters for DMRS [2].

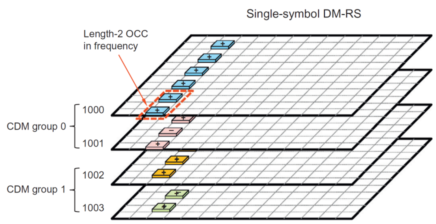

(a) Configuration type 1, single symbol DMRS.

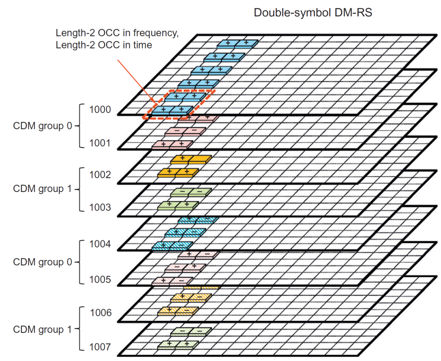

(b) Configuration type 1, double symbol DMRS.

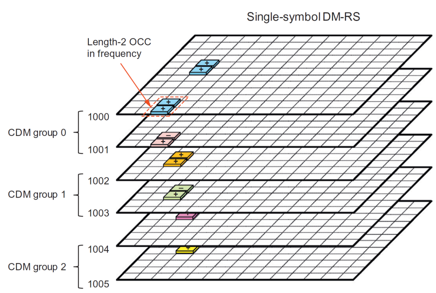

(c) Configuration type 2, single symbol DMRS.

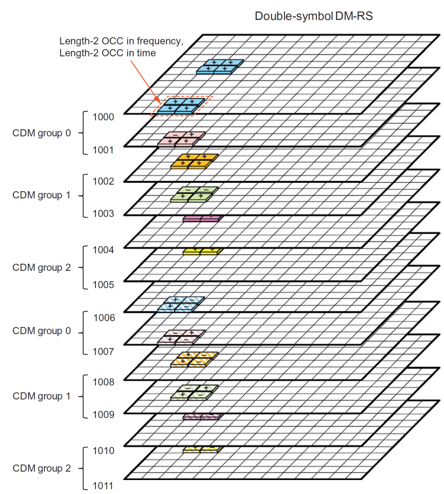

(d) Configuration type 2, double symbol DMRS.

Figure 1.3: DMRS locations in slot for different configuration parameters [2].

In addition, the effect of the $N_{\text{add}}^{\text{DMRS}}$ (additional position parameter) can be observed in Fig. 1.4 [2]. Namely, $N_{\text{add}}^{\text{DMRS}}$ determines the density of DMRS in time. For a 14 OFDM symbol length of the slot, at most 4 OFDM symbols can be allocated for DMRS transmission. Other configuration possibilities for double symbol and mapping type B can also be observed in the figure 1.3.

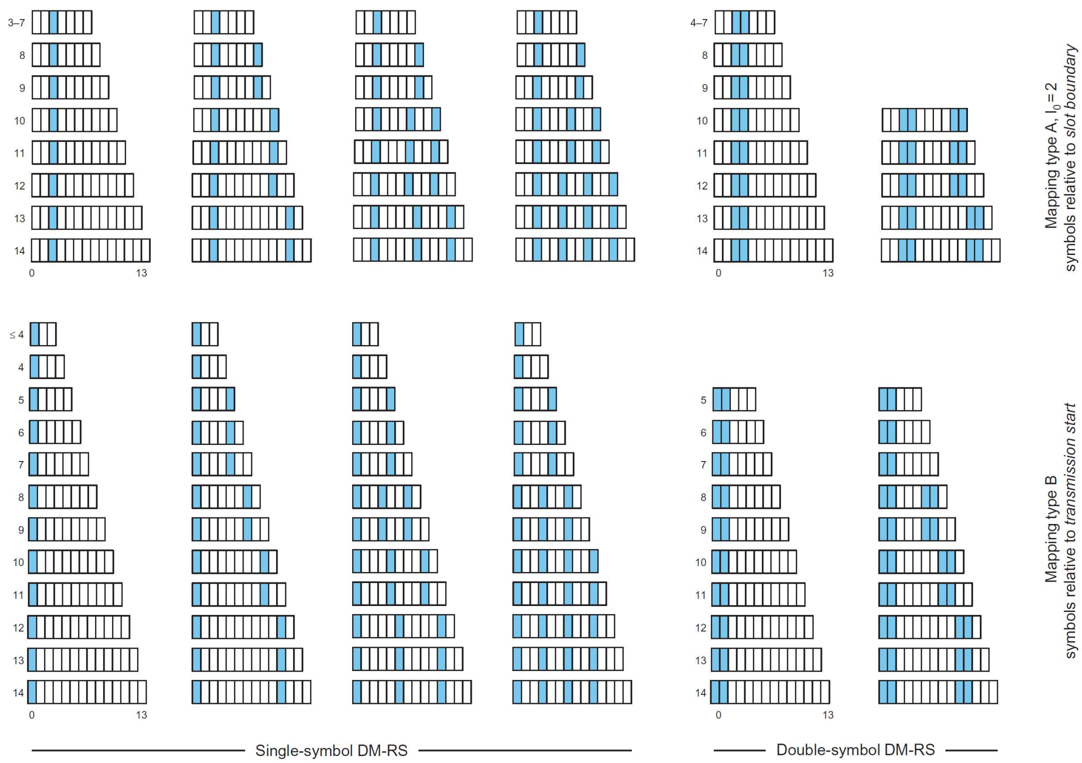

Figure 1.4: DMRS time locations for different configuration parameters [2].

1.3.2 Phase Tracking Reference Signal (PTRS) Structure

Phase tracking reference signal (PTRS) is used to estimate and compensate the oscillator phase noise for above-6 GHz bands in 5G. The PTRS structure provided in 5G NR is to compensate the CPE mainly. The CPE effect is identical for all subcarriers, but CPE has no significant correlation for adjacent OFDM symbols. Therefore, PTRS has a higher density in the time domain compared to the frequency domain resource allocation [15].

There are two main parameters that determine the PTRS configuration and resource allocation in the OFDM grid:

- **Time Density $d_{\textbf{time}}^{\textbf{PTRS}}$**: $d_{\text{time}}^{\text{PTRS}} \in \{1, 2, 4\}$ defines the time density of PTRS symbols on the OFDM grid. PTRS symbols are used once every $d_{\text{time}}^{\text{PTRS}}$

OFDM symbols.

- **Frequency Density $d_{\mathbf{freq}}^{\mathbf{PTRS}}$**: $d_{\text{freq}}^{\text{PTRS}} \in \{2, 4\}$ defines the frequency density of PTRS symbols on the OFDM grid. PTRS symbols are used once every $d_{\text{freq}}^{\text{PTRS}}$ resource blocks (consisting of 12 subcarriers) in the OFDM grid.

The PTRS configuration parameters can be decided according to the oscillator quality, carrier frequency, subcarrier spacing, and modulation and coding scheme (MCS). These are the main indicators of the significance of the phase noise on the performance degradation. Example configurations of PTRS for different additional DMRS uses are shown in Fig. 1.5.

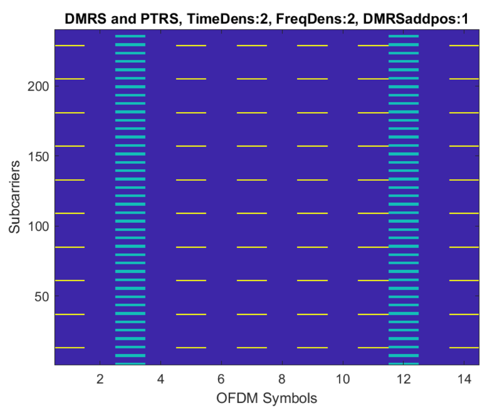

(a) PTRS configuration example.

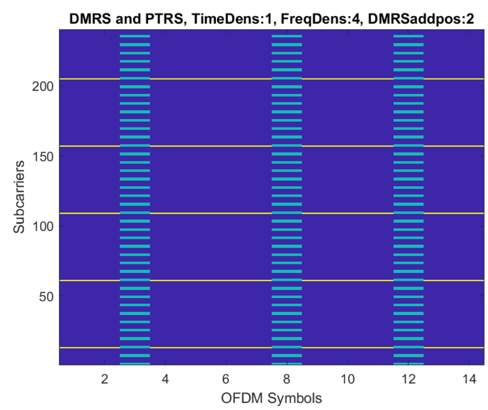

(b) PTRS configuration example.

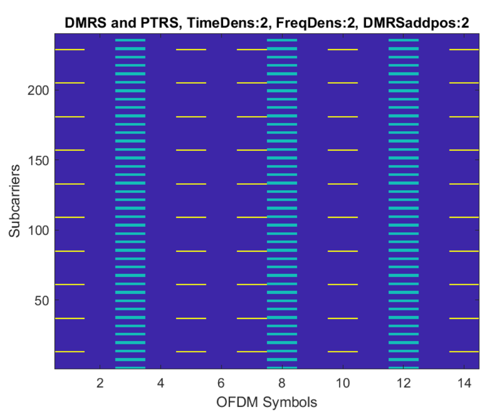

(c) PTRS configuration example.

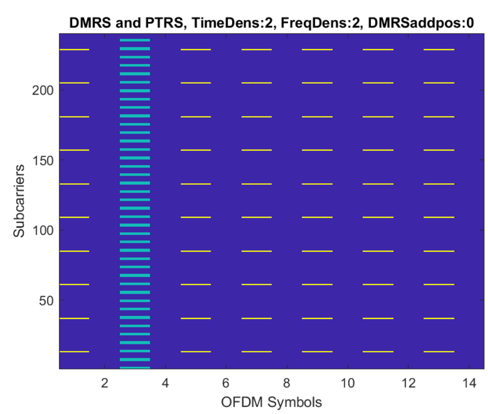

(d) PTRS configuration example.

Figure 1.5: OFDM grid generation examples in MATLAB for different PTRS time density and additional DMRS position parameters.

The QPSK modulated PTRS symbol for the kth subcarrier is determined as the DMRS symbol that is generated at the l_0th position in the time domain and the kth subcarrier in the frequency domain as explained in [14]. The PTRS is transmitted over one port only, which is associated with only one DMRS port.

1.4 Phase Noise

In wireless communications, the effects of the channel and the additive noise at the receiver side are the main causes that degrade the overall system performance. Moreover, the phase noise due to the oscillator components can be an important factor in some communication systems. In the case of 5G and mm-Wave, the system performance could be degraded significantly because of the phase noise introduced by the local oscillators, especially for higher carrier frequencies [16]. The effect of the phase noise can be observed in two parts: common phase error (CPE) and inter-carrier interference (ICI). When we consider the OFDM grid (frequency domain) at the receiver side, CPE represents a common phase rotation for each subcarrier. On the other hand, ICI mainly consists of the interference among adjacent subcarriers which cannot be ignored and should be dealt with especially when high modulation and coding scheme scenarios are considered [17]. The two main effects of the phase noise on the received signal constellation are illustrated in Fig. 1.6 [3].

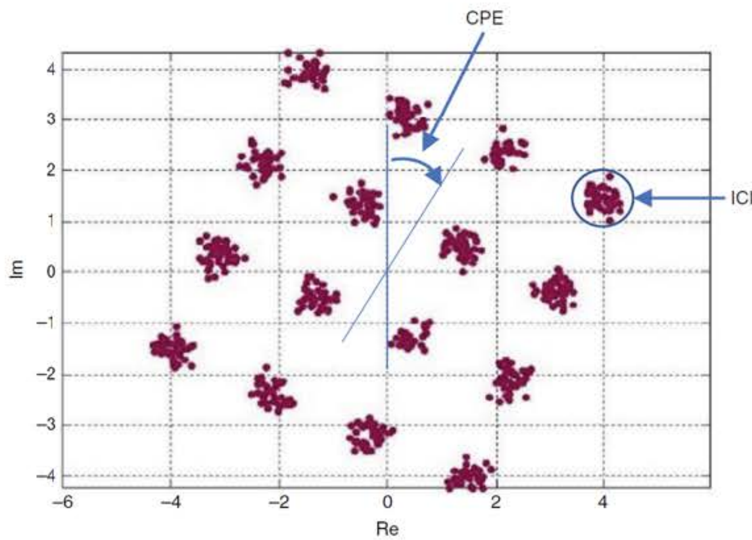

Figure 1.6: CPE and ICI effects on the received constellation [3].

1.5 Contribution of the Thesis

This thesis develops an end-to-end simulation environment for 5G physical downlink shared channel (PDSCH) to examine the system performance under channel and phase noise effects for mm-Wave communications (above 52.6 GHz). Reference signals (DMRS and PTRS) are generated according to the 3GPP 5G standards and used for channel and phase noise estimation. The effects of reference signal parameters for DMRS and PTRS on the system performance are observed jointly for different channel models in MATLAB. In the performance analysis, we do not assume the channel to be known during the simulations. We implement a SIMO system working at mm-Wave frequencies, which may seem controversial. However, we are interested in the channel and phase noise estimation performance to compare the performance of PTRS based channel estimation with DMRS based one, where for PTRS transmission, only one port can be used. Therefore, implementing a SIMO system can still enable us to obtain the desired results in a more practical way.

In addition to the application of different estimation algorithms, at the end of the simulations, this thesis proposes a PTRS based channel estimation for high Doppler scenarios. As we are working in mm-Wave, we propose both PN affected and PN free channel estimations to be performed over PTRS symbols. We also propose to double the maximum possible PTRS density in frequency domain. We show that PTRS based channel and phase noise estimation can outperform the conventional way of DMRS based channel estimation and PTRS based channel estimation for certain scenarios.

Chapter 2

System Model

This chapter defines the system model by explaining the phase noise generation process and signal model derivation considering the effects of channel and phase noise. Firstly, we explain the procedure to obtain analytical models for the phase noise signal in discrete-time from the proposed models on the power spectral density (PSD) of the phase noise. Then, we present the most up-to-date PSD models proposed for mm-Wave communications and used in 3GPP contribution reports. Finally, we provide the OFDM signal model together with the channel and phase noise effects on the received signal.

2.1 Phase Noise Modeling

In an ideal scenario, a perfect sinusoidal signal with a power spectrum of delta function at the carrier frequency could be produced by an oscillator. However, in practice, for both the transmitter and the receiver, local oscillators are not ideal and phase noise (PN) exist, which degrades the overall system performance. To investigate this situation and mitigate the PN effects, there should be a reliable statistical model so that one can develop robust estimation and compensation algorithms.

In the literature, there are mostly discrete-time models for the PN. For example, a simple model assuming that samples of random phases are distributed uniformly in the interval $[-\pi, \pi)$ is employed in [18]. Another possible model adopts Wiener random process to create correlation between the discrete-time samples in [19] and [20, 21] to represent a non-flat spectrum.

For a non-flat spectrum representation of the PN, several models for the PSD of the PN can be found, where the PSD samples in dBc/Hz are constructed by the direct measurements from real oscillators. Since the impact of PN is dependent on the oscillator performance and it can be modeled by the oscillator phase noise PSD, which implies that the discrete-time phase noise signal can be modeled by PSD properties. For the PSD representation of the PN, dBc/Hz is used for the phase noise ($\phi(t)$) or the phasor ($e^{j\phi(t)}$) power that is relative to the carrier frequency [22]. It can also be said that using the PSD models instead of random processes for phase noise generation results in more realistic simulations as the PSD models are proposed by observing the properties of state-of-the-art oscillators, especially for mm-Wave [23]. For a given PSD model of PN, an analytical approach to generate a discrete-time phase noise signal is explained in the following:

The time domain signal can be written as follows:

$$\begin{aligned} x(t) &= Re\{u(t)\exp\{j(2\pi f_c t + \phi(t))\}\} \\ &= Re\{u(t)\exp\{j\phi(t)\}\exp\{j2\pi f_c t\}\} \end{aligned} \tag{2.1}$$

where $\phi(t)$ represents the PN signal in time domain. For a given phase noise PSD $S_\phi(f)$, we want to generate $\phi(t)$. Let $w(t)$ be white Gaussian noise (WGN) for a basic filtering system as shown below:

$$\mathrm{w(t)} \longrightarrow \boxed{\mathrm{h(t)}} \longrightarrow \phi(t)$$

Here, $h(t)$ denotes the impulse response of the filter and the PSD of the WGN is given by $S_W(f) = N_0/2$ for all f. From this, the following equation can be derived:

$$S_\phi(f) = S_W(f)\,|H(f)|^2 \tag{2.2}$$

where $H(f)$ represents the frequency response of the filter. By simply manipulating this, $H(f)$ can be found as

$$H(f) = \sqrt{\frac{2}{N_0}}\sqrt{S_\phi(f)} \tag{2.3}$$

Applying the inverse Fourier transform on (2.3) gives $h(t)$ in the considered system as

$$h(t) = \mathcal{F}^{-1}\left\{\sqrt{\frac{2}{N_0}}\sqrt{S_\phi(f)}\right\} \tag{2.4}$$

Therefore, for a given phase noise PSD model $S_\phi(f)$ and $w(t)$ being AWGN, the time domain PN signal can be generated as follows:

$$\phi(t) = w(t) * h(t) \tag{2.5}$$

where $*$ denotes the convolution operator.

2.1.1 Phase Noise PSD and 3GPP Models

There are three main causes of the oscillator-based phase noise, which are the reference clock of the oscillator, phase-locked loop (PLL) components, and the voltage-controlled oscillator (VCO) [24].

For 5G mm-Wave, there are many models generated by the companies to achieve a realistic scenario. It is a common approach to use a multiple zero/pole model for phase noise PSD. A new phase noise model based on recently published data on both the state-of-the-art PLL and crystal oscillators is given by Ericsson, which is shown below:

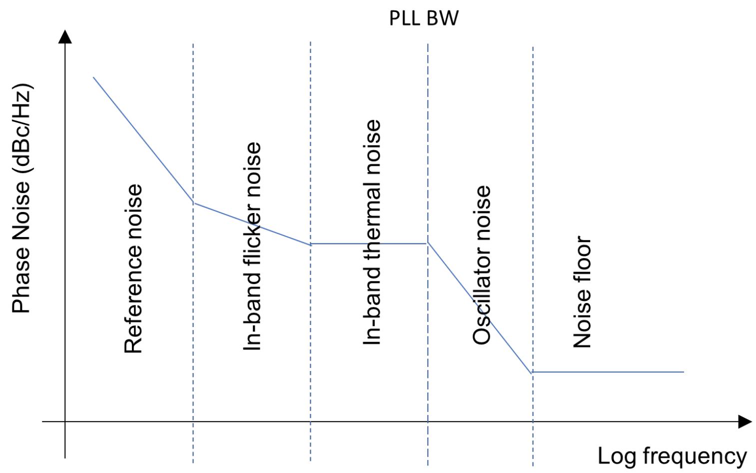

Figure 2.1: PLL phase noise mode for different frequency offsets [4].

In order to achieve such a PSD model, the multiple pole/zero model given below is used.

$$S(f_0) = PSD0\,\frac{\prod_{n=1}^{N}\left(1+\left(\frac{f_0}{f_{z,n}}\right)^{\alpha_{z,n}}\right)}{\prod_{m=1}^{M}\left(1+\left(\frac{f_0}{f_{p,m}}\right)^{\alpha_{p,m}}\right)} \tag{2.6}$$

The parameters for the poles and zeros for equation (2.6) are given in the table below:

Parameter	Value/expression	Parameter	Value
$PSD0$	$\left(\frac{f_c}{3.55e9}\right)^2 \cdot 10^{DM/10}$		
$f_{z,1}$	1.6e3	$\alpha_{z,1}$	2
$f_{z,2}$	200e3	$\alpha_{z,2}$	1
$f_{z,3}$	$\frac{f_c}{44.8}$	$\alpha_{z,3}$	2
$f_{p,1}$	1	$\alpha_{p,1}$	3
$f_{p,2}$	1e6	$\alpha_{p,2}$	2

The resulting phase noise PSD model is shown in Fig. 2.2 (black colored) together with many other models proposed by other companies [4].

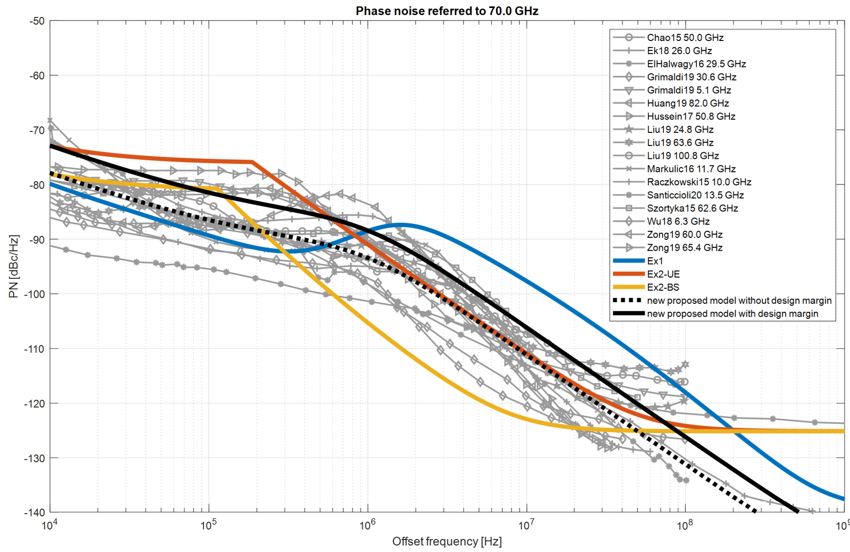

Figure 2.2: Phase Noise PSD models [4].

At this point, given the phase noise PSD model, the time domain phase noise can be found, as explained in the previous part. The general OFDM signal model can now be derived for the 5G PDSCH channel.

2.2 Signal Model

In this part, the OFDM signal model for 5G PDSCH is presented for one OFDM symbol duration with phase noise and channel effects. It is assumed that the channel does not change during one OFDM symbol duration. In the system model, N subcarriers with Δf_{sub} subcarrier spacing are used in one OFDM symbol. For a bandwidth of W, the sampling rate of the signal is $T_s = 1/W$. Let X_k represent the transmitted symbols on the kth subcarrier for $k = \{0, 1, 2, \ldots, N-1\}$. The OFDM symbol with a duration of $T = NT_s$ seconds can be found by applying an inverse discrete-time Fourier transform on X_k as follows:

$$x_n = \frac{1}{\sqrt{N}} \sum_{k=0}^{N-1} X_k e^{\frac{j2\pi kn}{N}}, \; n = 0, 1, 2, \ldots, N-1 \tag{2.7}$$

Let $\Phi = [\phi_0, \phi_1, \ldots, \phi_{N-1}]$ be the phase noise realization during one OFDM symbol, which can be constructed by sampling the time domain phase noise $\phi(t)$ given in equation (2.5) at time instances $t = nT_s$ for $n = 0, 1, 2, \ldots, N-1$. By including the channel effects, the received signal can be written as follows:

$$\mathbf{r} = diag\left(e^{j\Phi}\right)(\mathbf{x} \circledast \mathbf{h}) \tag{2.8}$$

where $\mathbf{x}$ is the OFDM signal as specified in (2.7), $\mathbf{h}$ is the channel impulse response, and $\circledast$ denotes the circular convolution operation. By applying FFT on $\mathbf{r}$, the received signal in the frequency domain can be given as

$$\mathbf{R} = \mathbf{J} \circledast (\mathbf{diag}(\mathbf{X})\,\mathbf{H}) \tag{2.9}$$

where $J_i = \frac{1}{N}\sum_{n=0}^{N-1} e^{j\phi_n} e^{\frac{-j2\pi ni}{N}}$ represents the frequency domain components of the ICI effect, and $\mathbf{X}$ and $\mathbf{H}$ are $N \times 1$ vectors representing the Fourier transforms of the time domain signals $\mathbf{x}$ and $\mathbf{h}$.

Denoting the additive WGN (AWGN) on the kth subcarrier as μ_k, the signal at the receiver side can be written as

$$R_k = \sum_{l=0}^{N-1} X_l H_l J_{k-l} + \mu_k \tag{2.10}$$

Here, to see the common phase error (CPE) and inter-carrier interference (ICI) effects of the phase noise clearly, equation 2.10 can be rewritten as follows.

$$R_k = X_k H_k \underbrace{J_0}_{\text{CPE}} + \underbrace{\sum_{l=0, l\neq k}^{N-1} X_l H_l J_{k-l}}_{\text{ICI}} + \mu_k \tag{2.11}$$

In this equation, J_0 represents the CPE effect, whereas $\sum_{l=0,l\neq k}^{N-1} X_l H_l J_{k-l}$ denotes the ICI effect of the phase noise on the received signal. Therefore, in the signal model, together with the channel effect, we also see two different effects of the phase noise. To improve the communication performance, the phase noise must be estimated and compensated together with the channel equalization.

Chapter 3

Channel and Phase Noise Estimation

In this chapter, algorithms and calculations used for channel and phase noise estimation and compensation are explained in detail. The algorithms and calculations are taken from different parts of the literature and merged for an end-to-end simulation to examine the system performance for 5G PDSCH with different possible system parameters and use case scenarios.

For an end-to-end system performance analysis, after performing signal and noise generation as explained in the previous chapter, calculations for channel estimation and phase noise compensation are performed at the receiver. The general structure of the system shown in Fig. 3.1 can be explained as follows: At the receiver side, firstly, channel estimation is performed. The purpose of this PN-affected channel estimation (phase noise being ignored) is to use these estimates for PN estimation. (This procedure is explained in the following sections.) In the literature, channel coefficients to be used for phase noise estimation are commonly assumed to be known to observe the effects of phase noise estimation on the system performance. In this thesis, only the maximum channel delay, Doppler shift, and the noise variance are assumed to be known, while estimation and compensation algorithms are performed at each stage. After the PN-affected channel estimation, phase noise estimation algorithms are executed. There are two main estimation/compensation methods to mitigate the phase noise which are common phase error (CPE) compensation and inter-carrier interference (ICI) compensation methods. The CPE compensation method is simpler, and it aims to correct the rotation of the constellation as shown in Fig. 1.6. On the other hand, the ICI compensation method aims both. CPE effect exists since it is a simpler method and can be sufficient in terms of the quality of service (QoS), especially for lower carrier frequencies and lower modulation and coding scheme (MCS). Then, channel estimation is performed after PN compensation in order to get the received symbols and perform decoding.

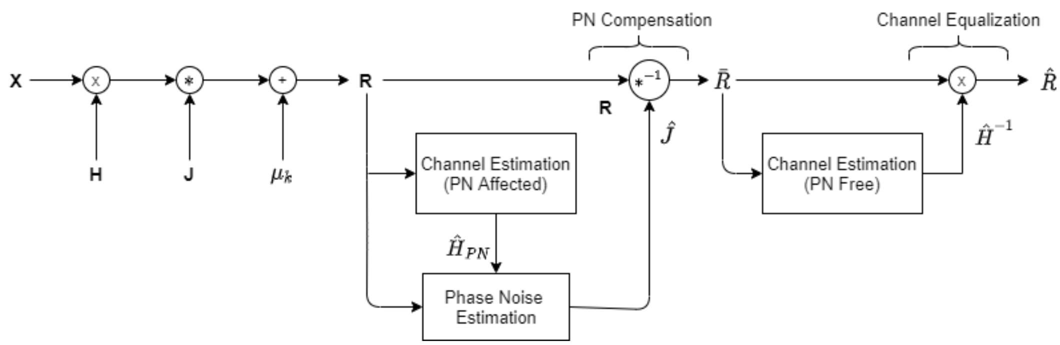

Figure 3.1: System model diagram.

In this section, firstly, the channel estimation technique is explained, and then the algorithms for phase noise estimation and compensation are investigated.

3.1 DMRS Based Channel Estimation

PN-affected channel estimation is performed before compensating the phase noise because initial channel estimates are needed for phase noise estimation. The channel estimation procedure, which is explained in this section, can be utilized for both PN-affected channel estimation and after, since in both cases, it is assumed that there is no effect of phase noise on the received signal.

For DMRS based channel estimation, firstly, least squares (LS) based channel estimation is performed on the DMRS carrying resource elements, and then based on these estimates, Wiener interpolation in two dimensions is applied to get the estimates of the channel for all resource elements in one slot duration. On the LS estimates of the channel, it is possible to use different interpolation techniques as linear interpolation, linear minimum mean-squared error (LMMSE) interpolation, and one dimensional Wiener filtering. However, in the literature, it is shown that two dimensional Wiener filtering/interpolation is mostly used since it can provide the best performance [25, 26, 27, 28].

The received signal model for an OFDM symbol with N samples in time domain is given as follows:

$$r[n] = \sum_{k=0}^{K-1} X(k)H(k)e^{\frac{j2\pi kn}{N}} + w[n],\ n = 0, 1, 2, \ldots, N-1 \tag{3.1}$$

where K is the number of subcarriers, $X(k)$ is the transmitted symbol at the kth subcarrier, $H(k)$ is the channel effect at the kth subcarrier, and $w[n]$ is the time domain additive noise. Here, the effect of phase noise is ignored for PN-affected channel estimation.

For this model, with l representing a resource element location on the OFDM grid, a simpler expression can be provided as follows:

$$R_l = X_l H_l + W_l \tag{3.2}$$

Let $\mathbf{P}_{slot} = \{l_0, l_1, \ldots, l_{N_p-1}\}$ represent the pilot carrying subcarriers along the frequency domain, where N_p is the number of pilot symbols in one slot. Then,

$$\mathbf{X}_{\mathbf{P}_{slot}} = \left[X_{l_j}\right],\ j = 0, 1, \ldots, N_p - 1 \tag{3.3}$$

denote the transmitted pilot symbols. Therefore, the LS channel estimates at $\mathbf{P}$ locations are calculated as follows [29, 30]:

$$\hat{\mathbf{H}}^{LS}_{\mathbf{P}_{slot}} = \left[\frac{R_{l_0}}{X_{l_0}}, \frac{R_{l_1}}{X_{l_1}}, \ldots, \frac{R_{l_{N_p-1}}}{X_{l_{N_p-1}}}\right]^T. \tag{3.4}$$

For N_p being the number of pilots sent in one slot duration, we write the LS channel estimate vector as follows:

$$\hat{\mathbf{H}}^{LS}(k) = \hat{H}_k,\ k = 1, \ldots, N_{P_l}. \tag{3.5}$$

3.1.1 Wiener Filtering

In order to obtain channel estimates for all resource elements in a slot, interpolation must be performed over the LS estimates of the channel on pilot carrying resource elements. For this purpose, $\mathbf{W}$ being an $(N_{sub}N_{sym}) \times N_p$ Wiener filter matrix and N_{sub} being the number of subcarriers during one OFDM symbol, the overall channel estimate in a slot can be calculated as follows [28]:

$$\hat{\mathbf{H}}^{MMSE} = \mathbf{W}\hat{\mathbf{H}}^{LS} \tag{3.6}$$

The 2D Wiener matrix in (3.6) can be calculated by the frequency-time domain autocorrelation matrices as follows:

$$\mathbf{W} = \mathbf{\Phi}(\mathbf{\Phi}_P + \sigma^2\mathbf{I}) \tag{3.7}$$

where σ^2 represents the noise variance that is assumed to be known.

First, the autocorrelation matrix in the frequency domain is calculated. For τ_{max} and N_p^{freq} being, respectively, the known maximum channel filter delay and the number of pilot symbols in one OFDM symbol duration, the $N_{sub} \times N_p^{freq}$ autocorrelation matrix in the frequency domain can be calculated as [28]

$$\phi_{freq}(k_1, k_2) = \sum_{i=0}^{\tau_{max}-1} \frac{1}{\tau_{max}} \exp\left[\frac{-j2\pi(k_2 - k_1)i}{N}\right] \tag{3.8}$$

For N_p^{time} being the number of OFDM symbols used for DMRS transmission in the time domain (i.e., $N_{add}^{DMRS} + 1$), the $N_{sym} \times N_p^{time}$ autocorrelation matrix in the time domain can be calculated as follows:

$$\phi_{time}(k_1, k_2) = \mathbf{J}_0\left(\Delta_f(k_2 - k_1)\right) \tag{3.9}$$

where $\Delta_f = 2\pi\mathbf{f}_d^{max}N/T_s$ with $\mathbf{f}_d^{max}$ denoting the maximum Doppler shift value in Hz.

We define $\mathbf{\Phi}_{freq}^P$ as the matrix constructed by the pilot carrying subcarrier indexed rows of the matrix $\mathbf{\Phi}_{freq}$ specified by (3.8). Also, let $\mathbf{\Phi}_{time}^P$ be the matrix that is constructed by the DMRS carrying OFDM symbol indexed rows of the matrix $\mathbf{\Phi}_{time}$ defined in (3.9). Then, the merged autocorrelation matrices for the 2D Wiener matrix calculations are expressed as follows:

$$\mathbf{\Phi} = \mathbf{\Phi}_{freq} \bigotimes \mathbf{\Phi}_{time} \tag{3.10}$$

$$\mathbf{\Phi}^P = \mathbf{\Phi}^P_{freq} \bigotimes \mathbf{\Phi}^P_{time} \tag{3.11}$$

Eventually, we can find the 2D Wiener filter $\mathbf{W}$ in equation (3.7) by using the frequency-time domain autocorrelation matrices [28].

3.2 Phase Noise Estimation and Compensation

As mentioned previously, for phase noise compensation, there are two main approaches as CPE compensation and ICI compensation. CPE compensation can be straightforward and effective in certain scenarios, whereas ICI mitigation algorithms are naturally more complex. There are two main approaches presented for ICI compensation in this thesis: de-ICI filtering and ICI approximation algorithm. The main idea behind these algorithms and their derivations are presented in the following sections.

It is important to note that each H_k term in the estimation algorithms below is the output of the PN-affected channel estimation (i.e., not assumed to be known), which is initially performed.

3.2.1 CPE Estimation and Compensation

In 5G, the PTRS structure in 3GPP Rel-15 is introduced to estimate the CPE [7]. For CPE estimation, the expression in (2.11) can be re-written as

$$R_k = X_k H_k J_0 + \epsilon_k\,, \quad k = 0, 1, 2, \ldots, N-1 \tag{3.12}$$

where ϵ_k is the new noise term, including the ICI component and AWGN noise. The objective function for the CPE estimation can be defined as [31]

$$\min_{J_0} \sum_{k \in P} |R_k - J_0 X_k H_k|^2 \tag{3.13}$$

By applying LS estimation on (3.13), an estimate of $\hat{J}_0$ can be found as

$$\hat{J}_0 = \frac{\sum_{k \in P} R_k X_k^* H_k^*}{\sum_{k \in P} |X_k H_k|^2} \tag{3.14}$$

After having an estimate of the CPE, its effect can be compensated as follows:

$$\hat{Y}_k = R_k \hat{J}_0^{\,*} \quad \text{for } k = 0, 1, 2, \ldots, N-1 \tag{3.15}$$

where $\hat{Y}_k$ is the estimate of the received symbol on the kth subcarrier for $k = 0, 1, 2, \ldots, N-1$.

After de-rotating the signal constellation, channel estimation and equalization can be performed prior to the demodulation of the received symbols.

3.2.2 ICI Estimation and Compensation

For higher carrier frequencies, the effect of the phase noise increases significantly, in which case the impact of ICI cannot be ignored [32]. Considering the 3GPP Rel-15 PTRS structure, this thesis presents two main approaches, which are explained in the following sections.

3.2.2.1 de-ICI Filtering

In de-ICI filtering, received symbols are used directly for the ICI filter estimation. For $u \geq 1$ being a positive integer, an ICI filter of length $2u+1$ is estimated. The advantage of de-ICI filtering is that it is well suited for the the Rel-15 PTRS structure. The symbols R_k around the pilot symbol are used directly (no knowledge of the transmitted signal is required), which is beneficial for simple implementation.

For X_k being the transmitted symbol on the kth subcarrier for $k \in \{0, 1, 2, \ldots, N-1\}$, let N_p be the number of PTRS symbols transmitted in an OFDM symbol. The pilot carrying subcarriers can be given as $\mathbf{P} = \{p_0, p_1, \ldots, p_{N_p-1}\}$. Given $\mathbf{P}$, $X_k = S_k$ can be written for $k \in \mathbf{P}$ since X_k is actually the transmitted PTRS symbol S_k for a pilot carrying subcarrier index.

Let a_m be the de-ICI filter of length $2u+1$. Then, the relation given below must be satisfied.

$$\sum_{m=-u}^{u} a_m R_{k-m} \approx H_k S_k \ , \ k \in P \tag{3.16}$$

where the objective function in (3.16) is given as follows:

$$\min_{a_m} \left\| \begin{bmatrix} R_{p_0+u} & R_{p_0+u-1} & \cdots & R_{p_0-u} \\ R_{p_1+u} & R_{p_1+u-1} & \cdots & R_{p_1-u} \\ \vdots & \vdots & \ddots & \vdots \\ R_{p_{N_p-1}+u} & R_{p_{N_p-1}+u-1} & \cdots & R_{p_{N_p-1}-u} \end{bmatrix} \begin{bmatrix} a_{-u} \\ a_{-u+1} \\ \vdots \\ a_u \end{bmatrix} - \begin{bmatrix} H_{p_0} S_{p_0} \\ H_{p_1} S_{p_1} \\ \vdots \\ H_{p_{N_p-1}} S_{p_{N_p-1}} \end{bmatrix} \right\|^2 \tag{3.17}$$

Here, the received symbols (depending on the filter size) around the PTRS carrying subcarriers are directly used for estimation. It can be seen that there is no need for a block PTRS structure. The equation above can be written as follows for simplification:

$$\min_{a_u} \left\| \mathbf{R}_u \mathbf{a}_u - \mathbf{x} \right\|^2 \tag{3.18}$$

Here, the LS estimate of the ICI filter $\mathbf{a}_u$ is calculated as [33]

$$\hat{\mathbf{a}}_{\mathbf{u}} = \left(\mathbf{R}_u^H \mathbf{R}_u \right)^{-1} \mathbf{R}_u^H \mathbf{x} \, . \tag{3.19}$$

After estimating the de-ICI filter, phase noise compensation is performed by filtering the received signal by $\hat{\mathbf{a}}_{\mathbf{u}}$ as follows:

$$\hat{Y}_k = [\mathbf{R} \circledast \hat{\mathbf{a}}_{\mathbf{u}}]_k \ \text{ for } k = 0, 1, 2, \ldots, N-1 \tag{3.20}$$

After phase noise compensation, the received signal is fed to the OFDM demodulator, where channel equalization and bit decisions are performed.

3.2.2.2 ICI Filter Approximation

The ICI filter approximation algorithm assumes that the block of transmitted symbols are known. It implies that one must use a block PTRS structure; however, it is still possible to employ this algorithm with the Rel-15 PTRS structure, with a return of increased complexity due to the iterative use of two algorithms (first CPE, then ICI estimation and compensation) and the process of making coarse decisions on the transmitted symbols. The receiver makes coarse decisions on the transmitted symbols around the PTRS carrying subcarriers so that these decisions can be used together with the PTRS symbol as a block of contiguous symbols to estimate an ICI filter of length $2u + 1$ for $u = 1, 2, \ldots$

For X_k being the transmitted symbol on the kth subcarrier for $k \in \{0, 1, 2, \ldots, N-1\}$, let N_p be the number of PTRS symbols transmitted in an OFDM symbol. The pilot carrying subcarriers can be given as $\mathbf{P} = \{p_0, p_1, \ldots, p_{N_p-1}\}$. Given $\mathbf{P}$, $X_k = S_k$ can be written for $k \in \mathbf{P}$, since X_k is actually the transmitted PTRS symbol S_k for a pilot carrying subcarrier index.

Let b_m be the de-ICI filter of length $2u+1$. Then, for $l = \{0, 1, 2, \ldots, N_p - 1\}$, defining $\{p_l - (M-1)/2, \ldots, p_l + (M-1)/2\}$ as the subcarrier indexes of the block of M (odd number) transmitted symbols, the following relation must be satisfied:

$$\sum_{m=-u}^{u} b_m H_{k-m} S_{k-m} \approx R_{k-m} \ , \ k \in \{p_l + (M-1)/2 + u, \ldots, p_l - (M-1)/2 - u\} \tag{3.21}$$

In order to write the objective function for equation (3.21), we let the following equations hold for $Z_{k-m} = H_{k-m}S_{k-m}$:

$$\mathbf{X}_u = \begin{bmatrix} Z_{p_l-(M-1)/2+2u} & Z_{p_l-(M-1)/2+2u-1} & \cdots & Z_{p_l-(M-1)/2} \\ Z_{p_l-(M-3)/2+2u} & Z_{p_l-(M-3)/2+2u-1} & \cdots & Z_{p_l-(M-3)/2} \\ \vdots & \vdots & \ddots & \vdots \\ Z_{p_l+(M-1)/2} & Z_{p_l+(M-1)/2-1} & \cdots & Z_{p_l+(M-1)/2-2u} \end{bmatrix}$$

$$\mathbf{b}_u = \begin{bmatrix} b_{-u} \\ b_{-u+1} \\ \vdots \\ b_u \end{bmatrix}$$

$$\mathbf{r}_u = \begin{bmatrix} R_{p_l-(M-1)/2} \\ R_{p_l-(M-1)/2+1} \\ \vdots \\ R_{p_l+(M-1)/2} \end{bmatrix}$$

Therefore, the objective function can be specified as follows:

$$\min_{b_u} \|\mathbf{X}_u\mathbf{b}_u - \mathbf{r}_u\|^2 \tag{3.22}$$

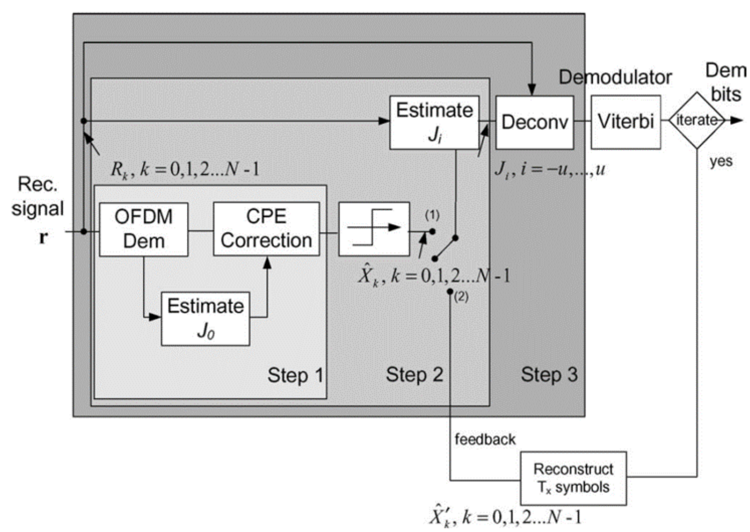

Figure 3.2: Data-aided ICI filter approximation algorithm [5].

To use the aforementioned algorithm with the Rel-15 PTRS structure, a data-aided system must be used. A simple and iterative algorithm for such a system can be found in the literature, as shown in Fig. 3.2. This algorithm can be implemented in four steps as follows:

- In Step 1, CPE estimation and compensation are performed as described in the previous section.
- After CPE compensation, rough decisions are made on the transmitted symbols to enable them for data-aid purposes.
- By using the aforementioned data symbols, ICI filter estimation, $\mathbf{b}_u$, and ICI compensation are performed.
- After ICI compensation, the algorithm can be performed iteratively, starting from Step 2.

An LS estimate of the ICI filter $\mathbf{b}_u$ in (3.22) can be calculated as follows [5]:

$$\hat{\mathbf{b}}_{\mathbf{u}} = \left(\mathbf{X}_u^H \mathbf{X}_u\right)^{-1} \mathbf{X}_u^H \mathbf{r}_u \, . \tag{3.23}$$

After estimating the ICI filter, phase noise compensation is performed by the de-convolution of filter $\hat{\mathbf{b}}_{\mathbf{u}}$ from the received signal as

$$\hat{Y}_k = [\mathbf{R} \circledast \hat{\mathbf{b}}_{\mathbf{u}}^*]_k \ , \quad k = 0, 1, 2, \ldots, N-1 \tag{3.24}$$

to get the received symbols Y_k.

After phase noise compensation, the received signal is fed to the OFDM demodulator, where channel equalization and bit decisions are performed.

3.3 Latest 3GPP Contribution Reports on PTRS and Phase Noise

In this section, we describe the latest contribution reports on how to enhance NR in terms of reference signal PTRS and phase noise estimation. In the reports, the current PTRS structure is evaluated, and expectations from the future contributions are stated.

Mainly, the focus is on two parts: PTRS design (resource allocation) and phase noise compensation algorithm. For the PTRS design, there are two options:

- Keep using Rel-15 PTRS design.
- Introduce a new design as block PTRS, using consecutive subcarriers in frequency domain PTRS symbols.

On the other hand, for the phase noise estimation algorithm, there are three main options as follows:

- CPE estimation and compensation algorithm.
- ICI estimation and compensation by de-ICI filtering algorithm.
- ICI estimation and compensation by ICI filter approximation algorithm.

In the following, among the possible discussion subjects regarding phase noise estimation and PTRS design, suggestions from companies are briefly summarized: In [34], above 52.6 GHz carrier frequencies, ICI becomes more dominant compared to CPE, and CPE compensation with the Rel-15 PTRS structure becomes unreliable. Therefore, ICI mitigation is crucial. For the same PTRS overhead, the Rel-15 structure can outperform a block PTRS structure. However, in the report, a cyclic sequence block design is proposed, in which case the use of a block PTRS can provide enhanced performance. Moreover, in [35], both theoretically and by simulations, it is shown that ICI compensation is necessary for higher MCS and carrier frequencies. Similar to [34], the use of a block PTRS structure with a cyclic-sequence is proposed.

Many contributions are suggesting that the use of a block PTRS is unnecessary. In [36] and [37], when ICI compensation is performed with the Rel-15 PTRS structure, results are similar to the block PTRS design for the same signaling overhead condition and complexity. In [38], the Rel-15 PTRS provides better performance with CPE, whereas the CPE method may not give a reliable performance for subcarrier spacing under 480 kHz. In [39], increasing the frequency domain density of the PTRS symbols (i.e., $d_{freq}^{PTRS} = 1$) does not contribute to the system performance. Furthermore, it is pointed out that block PTRS can occasionally collide with other reference signals such as CSI-RS and TRS. In [40], it is shown that for the 960 kHz subcarrier spacing, CPE compensation can provide similar performance results compared to ICI compensation where subcarrier spacing is 120 kHz. Therefore, from the preceding examples, many results and observations suggest that a new design of block PTRS is not necessary. In other words, the Rel-15 PTRS design must be preserved.

With the introduction of 52.6 GHz and above frequencies in 3GPP Rel-17, phase noise modeling, PTRS design, and phase noise estimation techniques are the subjects that are still to be investigated and standardized. For the current state of the standardization, according to the latest chairman's report, expectations from the companies to be studied and presented in the upcoming contribution reports can be summarized as follows [41]:

- Frequency density of PTRS, the structure of PTRS (Rel-15 or block or any other).
- Power boosting in frequency domain.
- Receiver complexity (for different algorithms) for both existing and potentially enhanced PTRS design (ICI compensation, filter size, etc).
- For block PTRS design, optimal block size and number of blocks to be used in the frequency domain with and without cyclic sequence.
- Maximum achievable spectral efficiency when PTRS overhead is concerned.

These are the subjects to be addressed and determined. Provided results will be evaluated based on performance benefits, receiver complexity, and specification efforts of the proposed algorithms and designs.

Chapter 4

Performance Analysis

Uncoded performance results for PDSCH are presented in this chapter. In the simulations, the performance of channel estimation is observed together with the phase noise compensation.

In the following sections, firstly, the optimal ICI filter lengths for direct de-ICI filtering and ICI filter approximation methods are chosen together with the optimal block length (M) for the ICI filter approximation method. Secondly, the effects of configuration parameter selections for DMRS and PTRS and the subcarrier spacing on the system performance are observed under different channel types (TDL-A and TDL-C) with varying channel delay spreads [14], [42]. Finally, the system and channel estimation performance is observed under high Doppler scenarios.

In the simulation results, "de-ICI" is used as an abbreviation for the direct de-ICI filtering method, "ICIclust" is used as an abbreviation for the ICI filter approximation method, and "CPE" is used as an abbreviation for the CPE compensation method.

4.1 PDSCH/PTRS Channel Equalization and Phase Noise Compensation Results

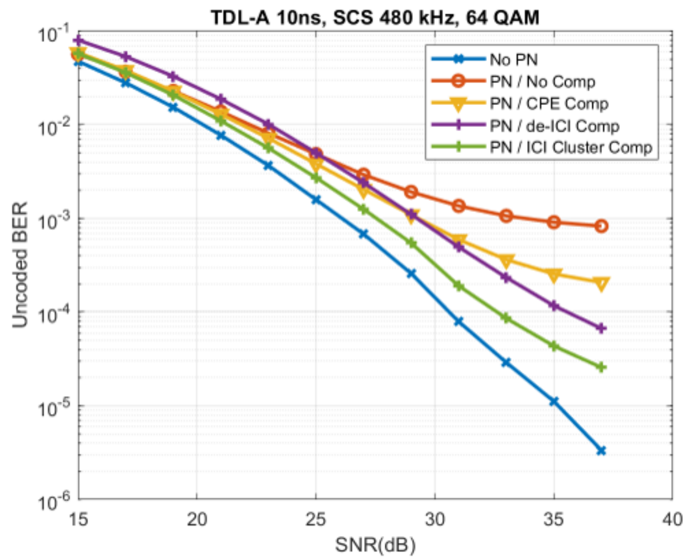

Figure 4.1: General comparison of the algorithms.

For the TDL-A channel with 10 ns delay spread, a general comparison of the algorithms is shown in Fig. 4.1 when 480 kHz subcarrier spacing is used. From the figure, it is observed that the ICIclust algorithm achieves the best performance but there is still a 2 dB loss compared to the case where there is no phase noise in the system. For higher SNRs, the de-ICI algorithm outperforms the CPE estimation. However, considering the lower complexity and improved performance of the CPE estimation method for low SNRs, it can be chosen over the de-ICI algorithm.

4.1.1 ICI Filter and Block Length Determination

For the ICIclust and de-ICI algorithms, performance comparisons for different ICI filter length selection and increased data block length for data-aided estimation of the phase noise are investigated in this part. First, the simulation parameters used for the results given in this section are shown in Table 4.1.

Simulation Parameters	
MIMO	1x2 SIMO
Monte Carlo Runs	100
Number of Bits Sent	25000
Carrier Frequency	70 GHz
Modulation	64-QAM (Uncoded)
User Speed	3 km/h
Subcarrier Spacing	240
Channel Type	TDL-A (MATLAB)
Channel Delay Spread	10 ns
Channel Estimation	LS Based 2D Wiener Filter Interpolation
Phase Noise Model	Ericsson Model [4]
DMRS Configuration Type	Type 1
$N_{\text{add}}^{\text{DMRS}}$	$\{0\}$
$d_{\text{time}}^{\text{PTRS}}$	1 (each symbol)
$d_{\text{freq}}^{\text{PTRS}}$	2 (once every 2 resource blocks)

Table 4.1: Simulation parameters for ICI filter and block length determination.

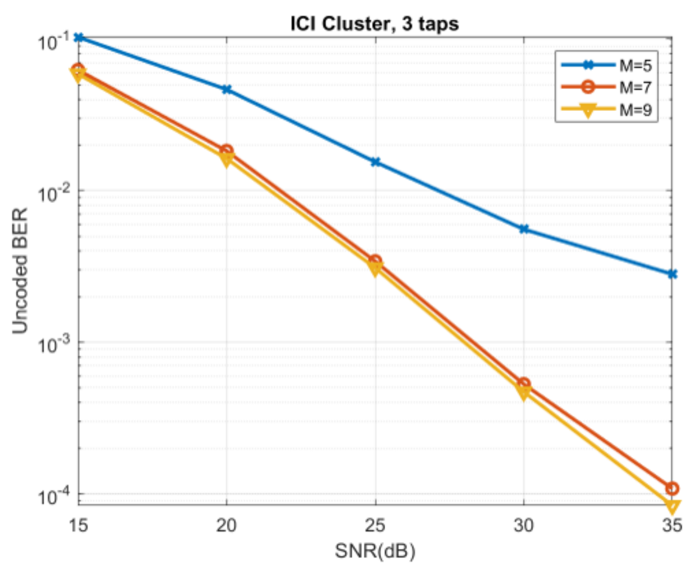

Figure 4.2: Performance results for ICIclust algorithm with ICI filter length of 3 for changing M.

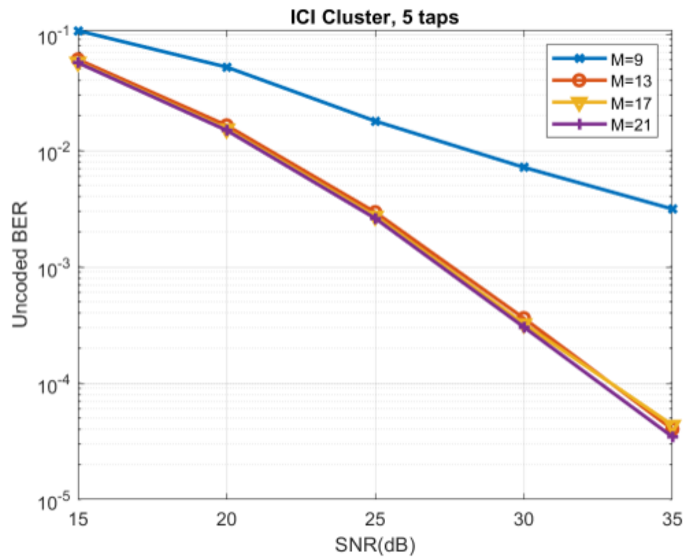

Figure 4.3: Performance results for ICIclust algorithm with ICI filter length of 5 for changing M.

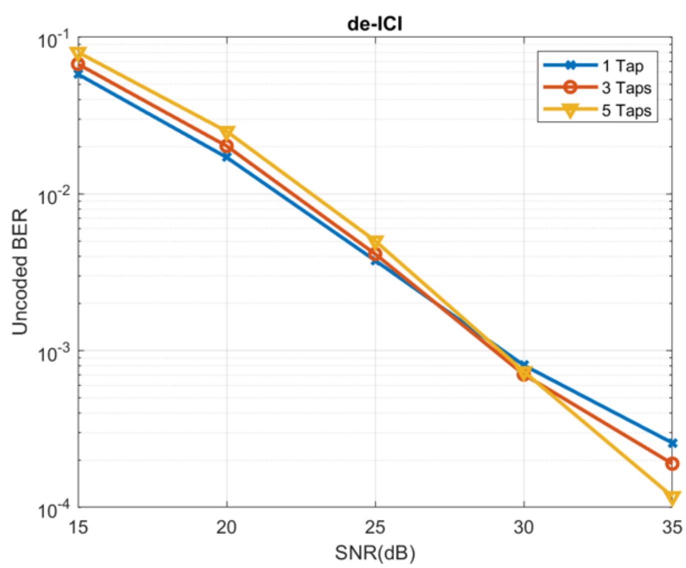

Figure 4.4: Performance results for de-ICI algorithm for changing ICI filter length.

In Figs. 4.2 and 4.3, the ICI filter length of 5 gives better performance as expected. Furthermore, for the ICI filter length of 5, increasing M over 13 has no significant contributions on the system performance. Therefore, for the ICIclust algorithm, the ICI filter length of $u = 5$ is used with the block length of $M = 13$ for enhanced performance results.

From Fig. 4.4, it can be observed that increasing the ICI filter length provides better system performance for higher SNR values whereas for lower SNRs, it degrades the overall system performance. The reason behind this result can be explained as the de-ICI algorithm being more prone to the additive noise compared to the ICIclust algorithm, since the received symbols are directly used at the receiver for phase noise estimation.

4.1.2 DMRS/PTRS Parameter Selection and Effect of Subcarrier Spacing

In this section, we investigate the effects of the configuration parameters of the reference signals and the subcarrier spacing on the overall system performance. The simulation parameters used for the results given in this section are shown in Table 4.2.

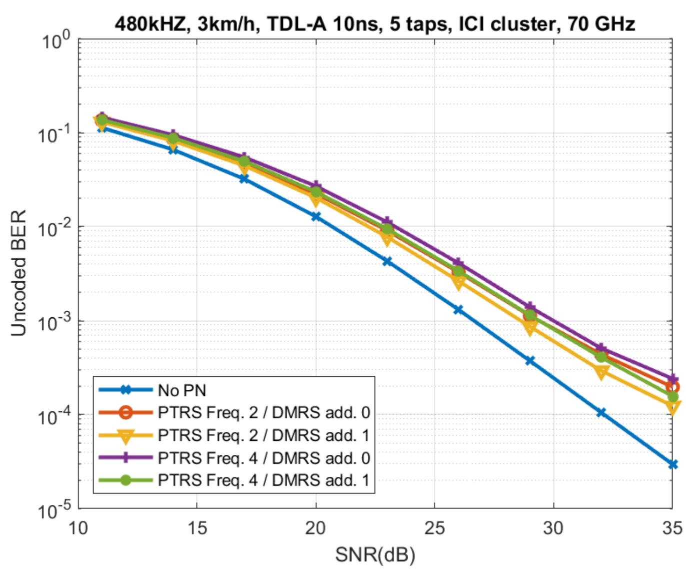

Figure 4.5: The effect of $N_{\text{add}}^{\text{DMRS}}$ and $d_{\text{freq}}^{\text{PTRS}}$ for 3 km/h user speed.

Simulation Parameters	
MIMO	1x2 SIMO
Monte Carlo Runs	100
Number of Bits Sent	25000
Carrier Frequency	70 GHz
Modulation	64-QAM (Uncoded)
User Speed	3 km/h, 30 km/h
Subcarrier Spacing	240 kHz - 480 kHz - 960 kHz
Channel Type	TDL-A (MATLAB)
Channel Delay Spread	5 ns - 10 ns
Channel Estimation	LS Based 2D Wiener Filter Interpolation
Phase Noise Model	Ericsson Model [4]
DMRS Configuration Type	Type 1
$N_{\text{add}}^{\text{DMRS}}$	$\{0, 1\}$
$d_{\text{time}}^{\text{PTRS}}$	1 (each symbol)
$d_{\text{freq}}^{\text{PTRS}}$	$\{2, 4\}$
ICI Filter Size	5

Table 4.2: Simulation parameters for DMRS/PTRS configuration selection and effect of subcarrier spacing.

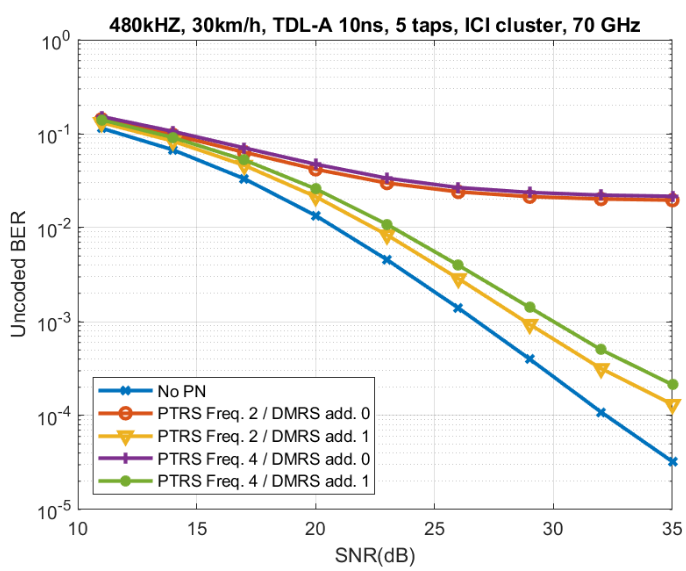

Figure 4.6: The effect of $N_{\text{add}}^{\text{DMRS}}$ and $d_{\text{freq}}^{\text{PTRS}}$ for 30 km/h user speed.

From Figs. 4.5 and 4.6, it can be seen that at least one additional DMRS symbol must be used for improved system performance. Furthermore, when additional

DMRS is used, increasing the frequency density of the PTRS can contribute to the system performance.

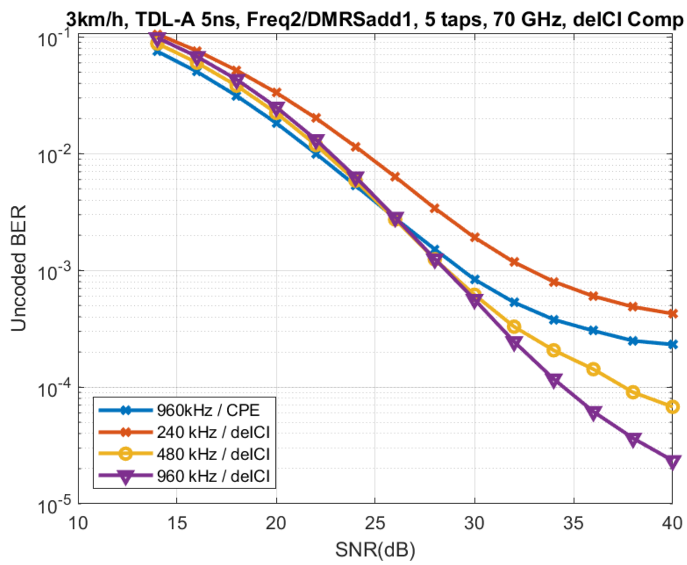

Figure 4.7: Performance results of different subcarrier spacing for direct de-ICI filtering algorithm.

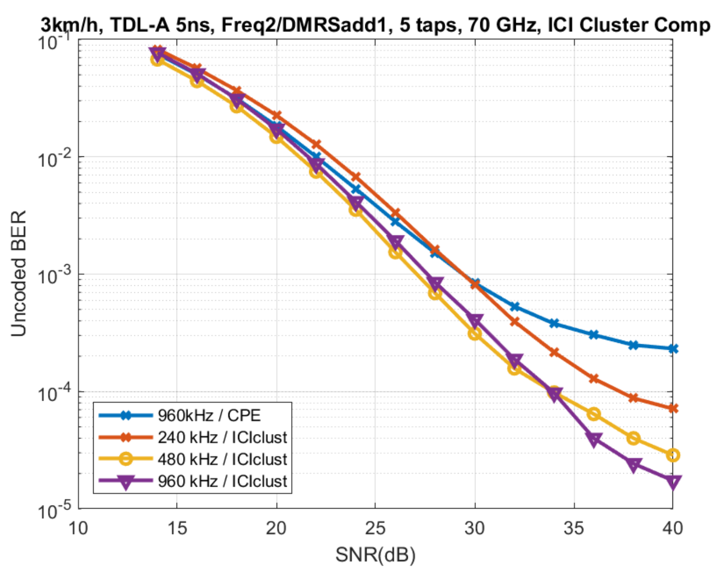

Figure 4.8: Performance results of different subcarrier spacing for ICI filter approximation algorithm.

In Figs. 4.7 and 4.8, the effects of subcarrier spacing on the system performance are observed. It is noted that the system performance is better for 480 kHz subcarrier spacing (especially for the ICI filter approximation), whereas there is no evidence of improvement when 960 kHz subcarrier spacing is used for the given simulation parameters. The reason behind this is that even for 5 ns of delay spread, there are paths in the TDL-A channel [14] which cause ISI. It can also be observed that increased subcarrier spacing is more beneficial for the de-ICI algorithm compared to the ICIclust.

It is important to emphasize that for the CPE estimation with 960 kHz of subcarrier spacing, the ICI suppression algorithms can outperform it even for lower subcarrier spacing values. This shows the importance and possible necessity of the ICI compensation for higher MCS.

4.2 DMRS and PTRS Based Channel Estimation Results for High Doppler Scenarios

In this section, channel estimation performance is evaluated in high Doppler scenarios for different channel delay profiles and delay spread values. The effect of additional DMRS use is also observed. Furthermore, for channel estimation, PTRS is used instead of DMRS to see whether it can be competent with the DMRS based channel estimation system. Note that when we say PTRS based channel estimation, only PTRS is used for the entire system from the beginning to the end. We also implement the system for an increased density of PTRS in frequency domain and present the related results in this section. The simulation parameters used for the results given in this section are shown in Table 4.3.

In the plots given in Fig. 4.9, for 480 kHz of subcarrier spacing and the TDL-C channel with 10 ns of delay spread, the effects of $N_{\text{add}}^{\text{DMRS}}$ and $d_{\text{freq}}^{\text{PTRS}}$ on the system performance are observed (in terms of the channel estimation MSE performance

Simulation Parameters	
MIMO	1x2 SIMO
Monte Carlo Runs	1000
Number of Bits Sent	25000
Carrier Frequency	70 GHz
Modulation	64-QAM (Uncoded)
User Speed	60 km/h, 120 km/h, 180 km/h
Subcarrier Spacing	480 kHz
Channel Type	TDL-C (MATLAB)
Channel Delay Spread	5 ns - 10 ns
Channel Estimation	LS Based 2D Wiener Filter Interpolation
Phase Noise Model	Ericsson Model [4]
DMRS Configuration Type	Type 1
$N_{\text{add}}^{\text{DMRS}}$	{0, 1, 2, 3}
$d_{\text{time}}^{\text{PTRS}}$	1 (each symbol)
$d_{\text{freq}}^{\text{PTRS}}$	{1 (dense PTRS), 2}
ICI Filter Size	5

Table 4.3: Simulation parameters for high Doppler scenarios with DMRS and PTRS based channel estimation.

and the uncoded BER performance of the overall system) for the ICIclust algorithm. When the user speed is above $60km/h$, the use of at least one additional DMRS drastically improves the system performance. For above $180km/h$ user speed, it is best to use two additional DMRS for guaranteed performance. Moreover, the results for the PTRS based channel estimation are illustrated. It is important to note that we use increased PTRS density only for PTRS based channel estimation where we use no additional DMRS in the system. For 10 ns of delay spread, PTRS based channel estimation cannot provide any reliable performance results just like DMRS based channel estimation with no additional DMRS. However, when the PTRS density in the frequency domain is doubled (i.e., $d_{\text{freq}}^{\text{PTRS}} = 1$), PTRS based channel estimation provides the best performance for all user speed and SNR values.

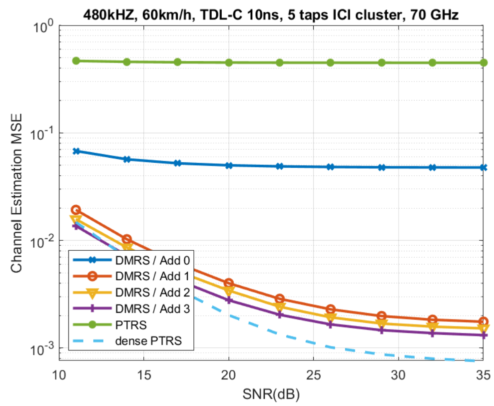

(a) Channel estimation MSE for 60 km/h.

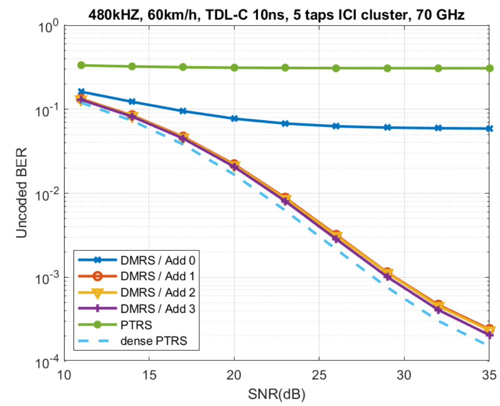

(b) Uncoded BER for 60 km/h.

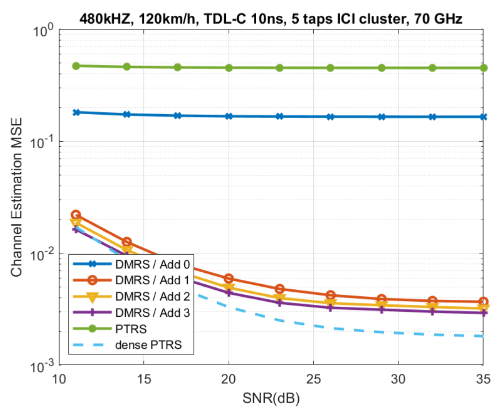

(c) Channel estimation MSE for 120 km/h.

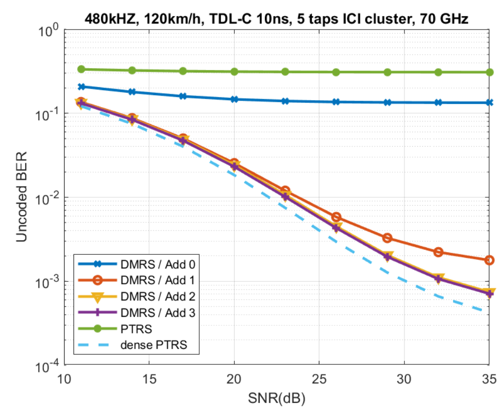

(d) Uncoded BER for 120 km/h.

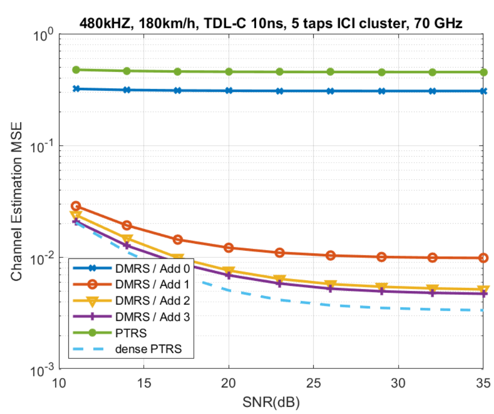

(e) Channel estimation MSE for 180 km/h.

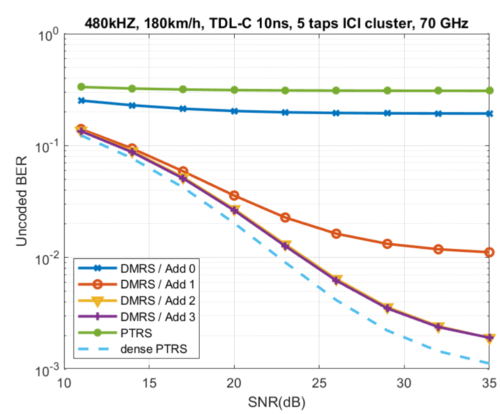

(f) Uncoded BER for 180 km/h.

Figure 4.9: Channel estimation MSE and uncoded BER performance results for high Doppler TDL-C channel with 10 ns of delay spread.

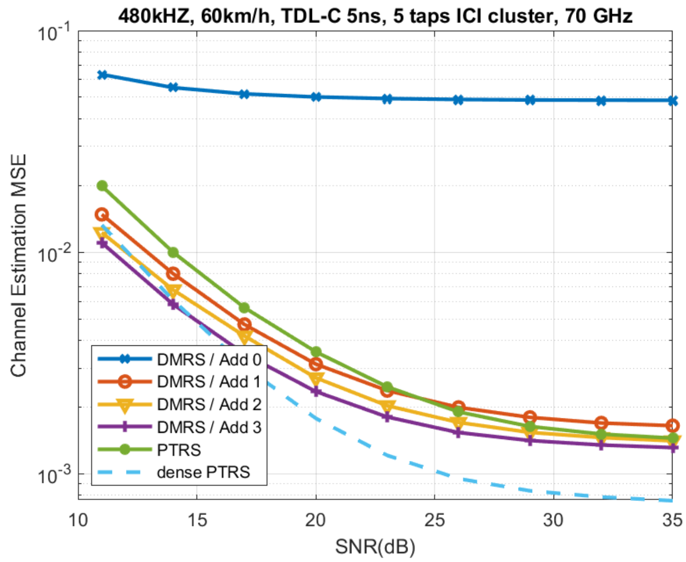

Figure 4.10: Channel estimation MSE for TDL-C channel with 5 ns of delay spread for 60 km/h user speed.

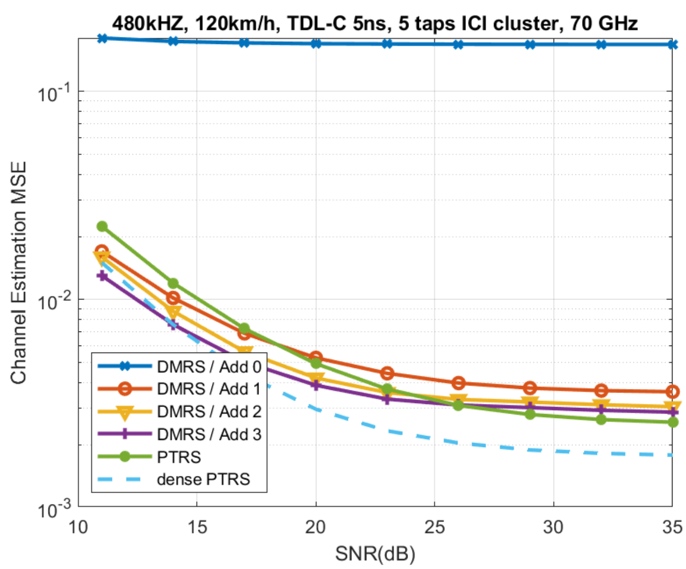

Figure 4.11: Channel estimation MSE for TDL-C channel with 5 ns of delay spread for 120 km/h user speed.

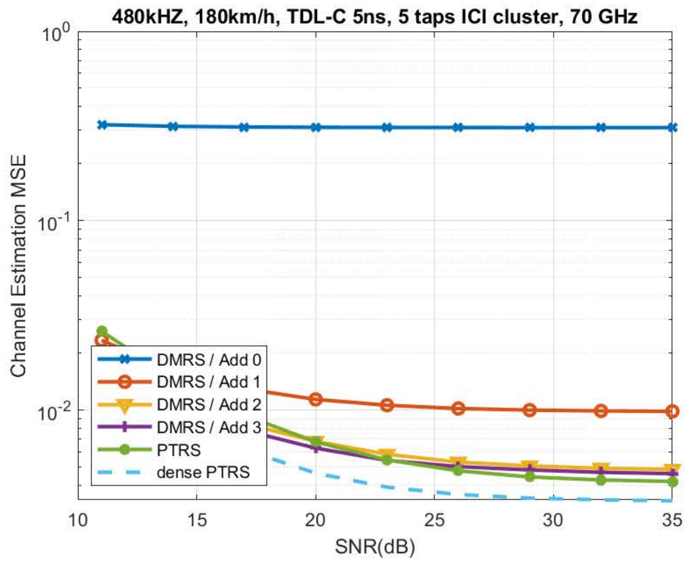

Figure 4.12: Channel estimation MSE for TDL-C channel with 5 ns of delay spread for 180 km/h user speed.

In Figs. 4.10–4.12, for 480 kHz of subcarrier spacing and the TDL-C channel with 5 ns of delay spread, the effects of $N_{\text{add}}^{\text{DMRS}}$ and $d_{\text{freq}}^{\text{PTRS}}$ on the system performance are observed for the ICIclust algorithm. Here, we look for the results in a lower delay spread channel to see if the PTRS based channel estimation without increased density could become competent with the DMRS based channel estimation in certain scenarios. From the figures, similarly to the previous cases but for a lowered delay spread channel this time, when the user speed is above $60km/h$, the use of at least one additional DMRS drastically improves the system performance. For above $180km/h$ user speed, it is best to use two additional DMRS for guaranteed performance. For lowered delay spread channel, the use of PTRS based channel estimation with increased density still provides the best overall performance, except for certain scenarios with low SNR values. On the other hand, for the Rel-15 PTRS, the PTRS based channel estimation is competent with the DMRS based channel estimation especially for increased user speeds.

Chapter 5

Conclusions and Future Work

In this thesis, we have first briefly explained the mm-Wave and evolution of mobile communications to 5G. We have discussed the current progress of 3GPP in mm-Wave communications and expectations from communications above 52.6 to 114.25 GHz. Additionally, the latest contribution reports on phase noise estimation algorithms and possibly enhanced PTRS designs have been presented. Then, 5G numerology and frame structure have been briefly explained together with the new aspects of 5G communications. Then, we have explained the structure of 5G PDSCH with its reference signals, DMRS and PTRS, where the effect of configuration parameters for DMRS and PTRS have been shown and illustrated. In addition, we have showed the effects of phase noise in OFDM systems, and analytical modeling of discrete-time phase noise with its PSD properties. Then, a general OFDM signal model has been shown with CPE and ICI effects caused by PN on the received signal. After generating the signal model, channel and phase noise estimation techniques have been explained in detail. The algorithms in the literature have been applied on 5G PDSCH and reference signal designs for simulating the system performance under multi-path channel and phase noise effects.

For channel equalization, a DMRS based channel estimation has been implemented with 2-D Wiener filtering. Two main approaches have been adopted for phase noise compensation: CPE and ICI compensation, where for ICI compensation, de-ICI filtering and ICI filter approximation techniques have been explained and performed. Each algorithm has been applied to the system to be used with the current PTRS design adopted by 3GPP Rel-15. For CPE and ICI filter estimations, it is also possible to derive and use MMSE estimation, however, due to the practicality (complexity) concerns, LS estimators are used. As future work, the detailed analysis should be performed for complexity calculations for different algorithms and PTRS designs.

To evaluate the system performance under different numerologies, reference signal configurations, and phase noise compensation algorithms, uncoded bit error rate (BER) plots have been generated so that the effects of these variables could be seen more clearly. We have performed simulations at 70 GHz, as 3GPP decides that further studies and simulations are required for communications above 52.6 to 114.25 GHz [11].

In the simulations, comparisons of all algorithms have been presented for the TDL-A channel together with the effects of subcarrier spacing on the performance. The effects of configuration parameter selections for DMRS and PTRS (PTRS frequency density and DMRS time density) on the system performance have also been illustrated. Then, for the high Doppler TDL-C channel, we have compared two cases where we have used the conventional system and a system where only PTRS signals have been used (both for channel and phase noise estimation). We have also increased the PTRS density further than it is possible in the current 5G standards (i.e., $d_{\text{freq}}^{\text{PTRS}} = 1$) for PTRS to be able to compete with DMRS considering the channel estimation performances. The results have shows that for high Doppler scenarios, using PTRS only is possible for reliable system performance for TDL-C channel with 5 ns of delay spread. On the other hand, for the results with 10 ns of delay spread, an increased PTRS density must be used for Rel-15 PTRS to be competent with DMRS.

As mentioned in the previous chapters, for communications above 52.6 to 114.25 GHz, possible enhancements on PTRS design and PN estimation algorithms are still being discussed. In contrast with the Rel-15 PTRS design, the primary approach uses a block PTRS in the frequency domain. As future work, theoretical bounds can be derived for specific scenarios to comprehend how good the possible reference signal designs are. Furthermore, machine learning techniques can be implemented for both channel and phase noise estimations individually.

Bibliography

[1] X. Lin, J. Li, R. Baldemair, J.-F. T. Cheng, S. Parkvall, D. C. Larsson, H. Koorapaty, M. Frenne, S. Falahati, A. Grovlen, *et al.*, “5G new radio: Unveiling the essentials of the next generation wireless access technology,” *IEEE Communications Standards Magazine*, vol. 3, no. 3, pp. 30–37, 2019.

[2] E. Dahlman, S. Parkvall, and J. Skold, *5G NR: The next generation wireless access technology.* Academic Press, 2018.

[3] M. Enescu, *5G New Radio: A beam-based air interface.* John Wiley & Sons, 2020.

[4] Ericsson, “On 52.6 to 71 GHz phase noise characteristics,” Tech. Rep. R4-2010176, 3GPP TSG-RAN WG4 96-E, August 2020.

[5] D. Petrovic, W. Rave, and G. Fettweis, “Effects of phase noise on OFDM systems with and without PLL: Characterization and compensation,” *IEEE Transactions on communications*, vol. 55, no. 8, pp. 1607–1616, 2007.

[6] T. M. B. Standard, “3GPP website.” (https://www.3gpp.org/, cited August 2021.).

[7] 3GPP, “NR physical layer procedure for data,” Tech. Rep. TS 38.214, 3GPP TSG RAN.

[8] F. Boccardi, R. W. Heath, A. Lozano, T. L. Marzetta, and P. Popovski, “Five disruptive technology directions for 5G,” *IEEE communications magazine*, vol. 52, no. 2, pp. 74–80, 2014.

[9] S. Rangan, T. S. Rappaport, and E. Erkip, "Millimeter-wave cellular wireless networks: Potentials and challenges," *Proceedings of the IEEE*, vol. 102, no. 3, pp. 366–385, 2014.

[10] S. Akoum, O. El Ayach, and R. W. Heath, "Coverage and capacity in mmWave cellular systems," in *2012 conference record of the forty sixth Asilomar conference on signals, systems and computers (ASILOMAR)*, pp. 688–692, IEEE, 2012.

[11] 3GPP, "Study on NR beyond 52.6 GHz," Tech. Rep. TR 38.807 V1.0.0, 3GPP TSG RAN.

[12] I. Corporation, "New SID: Study on supporting NR from 52.6GHz to 71 GHz," Tech. Rep. RP-193259, 3GPP TSG-RAN Meeting 82, December 2019.

[13] Qualcomm, "New WID on extending current NR operation to 71 GHz," Tech. Rep. RP-193229, 3GPP TSG-RAN Meeting 82, December 2019.

[14] 3GPP, "NR physical channels and modulation," Tech. Rep. TS 38.211, 3GPP, April 2018.

[15] S. Ahmadi, *5G NR: Architecture, technology, implementation, and operation of 3GPP new radio standards.* Academic Press, 2019.

[16] C. Johnson, *5G New Radio in Bullets.* Independently published, 2019.

[17] Y. Qi, M. Hunukumbure, H. Nam, H. Yoo, and S. Amuru, "On the phase tracking reference signal (PTRS) design for 5G new radio (NR)," in *2018 IEEE 88th Vehicular Technology Conference (VTC-Fall)*, pp. 1–5, IEEE, 2018.

[18] M. Katz and S. Shamai, "On the capacity-achieving distribution of the discrete-time noncoherent and partially coherent AWGN channels," *IEEE Transactions on Information Theory*, vol. 50, no. 10, pp. 2257–2270, 2004.

[19] G. Colavolpe, A. Barbieri, and G. Caire, "Algorithms for iterative decoding in the presence of strong phase noise," *IEEE Journal on selected areas in communications*, vol. 23, no. 9, pp. 1748–1757, 2005.

[20] H. Ghozlan and G. Kramer, "On Wiener phase noise channels at high signal-to-noise ratio," in *2013 IEEE International Symposium on Information Theory*, pp. 2279–2283, IEEE, 2013.

[21] H. Ghozlan and G. Kramer, "Models and information rates for Wiener phase noise channels," *IEEE Transactions on Information Theory*, vol. 63, no. 4, pp. 2376–2393, 2017.

[22] A. Demir, "Computing timing jitter from phase noise spectra for oscillators and phase-locked loops with white and $1/f$ noise," *IEEE Transactions on Circuits and Systems I: Regular Papers*, vol. 53, no. 9, pp. 1869–1884, 2006.

[23] A. Piemontese, G. Colavolpe, and T. Eriksson, "Phase noise in communication systems: from measures to models," *arXiv preprint arXiv:2104.07264*, 2021.

[24] Nokia, "On the evaluation of PN model," Tech. Rep. R1-165005, 3GPP TSG-RAN WG1 85, May 2016.

[25] J.-J. Van De Beek, O. Edfors, M. Sandell, S. K. Wilson, and P. O. Borjesson, "On channel estimation in OFDM systems," in *1995 IEEE 45th Vehicular Technology Conference. Countdown to the Wireless Twenty-First Century*, vol. 2, pp. 815–819, IEEE, 1995.

[26] M. Liu, M. Crussiere, and J.-F. Hélard, "Enhanced two-dimensional data-aided channel estimation for TDS-OFDM," in *2010 4th international conference on signal processing and communication systems*, pp. 1–7, IEEE, 2010.

[27] P. Hoeher, S. Kaiser, and P. Robertson, "Two-dimensional pilot-symbol-aided channel estimation by Wiener filtering," in *1997 IEEE international conference on acoustics, speech, and signal processing*, vol. 3, pp. 1845–1848, IEEE, 1997.

[28] V. Srivastava, C. K. Ho, P. H. W. Fung, and S. Sun, "Robust MMSE channel estimation in OFDM systems with practical timing synchronization," in *2004 IEEE Wireless Communications and Networking Conference (IEEE Cat. No. 04TH8733)*, vol. 2, pp. 711–716, IEEE, 2004.

[29] K. Zhang, L. Xue, X. Liu, and X. Chen, "Performance comparison of LS, LMMSE channel estimation method in frequency and time domain for OQAM/OFDM systems," in *2017 IEEE 17th International Conference on Communication Technology*, pp. 224–228, 2017.

[30] Y. Shen and E. Martinez, "Channel estimation in OFDM systems," *Freescale semiconductor application note*, pp. 1–15, 2006.

[31] P. Robertson and S. Kaiser, "Analysis of the effects of phase-noise in orthogonal frequency division multiplex (OFDM) systems," in *Proceedings IEEE International Conference on Communications ICC'95*, vol. 3, pp. 1652–1657, IEEE, 1995.

[32] S. Gu, H. Long, and Q. Li, "Phase noise estimation and compensation algorithms for 5G systems," in *International Conference on Communications and Networking in China*, pp. 551–561, Springer, 2018.

[33] Ericsson, "On phase noise compensation for OFDM," Tech. Rep. R1-2005922, 3GPP TSG-RAN WG1 102-E, August 2020.

[34] M. Electric, "PTRS enhancements for NR from 52.6GHz to 71GHz," Tech. Rep. R1-2100553, 3GPP TSG-RAN WG1 104-E, February 2021.

[35] Huawei, "PDSCH/PUSCH enhancements for 52-71 GHz band," Tech. Rep. R1-2100201, 3GPP TSG-RAN WG1 104-E, February 2021.

[36] ZTE, "Discussion on the data channel enhancements for 52.6 to 71GHz," Tech. Rep. R1-2101819, 3GPP TSG-RAN WG1 104-E, February 2021.

[37] FUTUREWEI, "Considerations for higher SCS support in beyond 52.6 GHz," Tech. Rep. R1-2100050, 3GPP TSG-RAN WG1 104-E, February 2021.

[38] Nokia, "PDSCH/PUSCH enhancements," Tech. Rep. R1-2100261, 3GPP TSG-RAN WG1 104-E, February 2021.

[39] Ericsson, "PDSCH/PUSCH enhancements," Tech. Rep. R1-2101310, 3GPP TSG-RAN WG1 104-E, February 2021.

[40] Q. Incorporated, “PDSCH and PUSCH enhancements for 52.6-71GHz band,” Tech. Rep. R1-2101457, 3GPP TSG-RAN WG1 104-E, February 2021.

[41] M. Support, “Draft report of 3GPP TSG RAN WG1 104bis-e v0.1.0,” Tech. Rep. R1-2101819, 3GPP TSG-RAN WG1 Meeting 104-E, May 2021.

[42] 3GPP, “5G Study on channel model for frequencies from 0.5 to 100 GHz,” Tech. Rep. TS 38.901, 3GPP.